Quantification of myocardial blood flow and flow reserve: Technical aspects

Ran Klein, PhD, Rob S. B. Beanlands, MD, and Robert A. deKemp, PhD

INTRODUCTION

Myocardial perfusion imaging (MPI) is a powerful tool for detection of impaired myocardial blood supply due to atherosclerotic lesions in the epicardial arteries. MPI is commonly conducted using single photon emission computed tomography (SPECT) with ^{201}Tl- or ^{99m}Tc-based tracers, under conditions of rest and hyperemic stress. Regions of high tracer uptake are assumed to be normally perfused, while regions with *relatively* low uptake (perfusion defects) typically reflect stenosis of the upstream arteries. Regions of reversible myocardial ischemia are identified as stress perfusion defects that normalize at rest.

In recent years, positron emission tomography (PET) has been utilized increasingly for MPI due to its superior image quality. PET images can be corrected accurately for attenuation losses and may have higher diagnostic accuracy than SPECT.[1-3] Attenuation effects are particularly important in overweight patients, women with large or dense breast tissue and men with high abdominal fat. Thus, PET MPI is generally accepted to have improved specificity (fewer false-positives) compared to SPECT MPI, and fewer inconclusive exams, especially in obese patients and in women.[4] Furthermore PET images provide quantitative measurements of activity concentration, and dynamic imaging can be used to quantify myocardial blood flow (MBF) in absolute terms of mL/minute/g.[5,6] This provides an added quantitative dimension to routine MPI, and is sensitive to disease in both the epicardial conduit vessels as well as the resistance vessels of the microvasculature.[7] MBF quantification has been shown to be beneficial in detecting multivessel disease that can cause a global reduction in flow, producing false-negative results with standard relative MPI.[8-12] In addition, MBF has been shown to detect subclinical or presymptomatic disease in the microvasculature[13-15] in diabetes, hypertension, hyperlipidemia, and obesity.[16-18]

Routine perfusion imaging uses radio-labeled tracers that are extracted from the blood and retained by the myocardium, ideally in proportion to blood flow. The net tracer concentration (uptake) in the tissue is therefore related to the rate of blood supply. As opposed to MPI which uses static images of the relative tracer distribution following blood clearance, MBF quantification uses dynamic sequences of images measured during the entire tracer uptake and clearance phases. Time-activity-curves (TAC) are measured in arterial blood and in regions of myocardial tissue. A tracer kinetic model is used to describe the exchange of tracer between arterial blood and myocardium during the course of the scan. In particular, the rate of tracer uptake (transport) from blood to tissue is closely related to MBF, depending only on the tracer extraction fraction.

This article describes the technical considerations associated with MBF quantification with PET, mainly using the MPI tracers ^{82}Rb and ^{13}N-ammonia, and quality assurance methods needed to ensure clinical measurements of high quality.

PERFUSION TRACERS

The properties of clinically applicable perfusion tracers are shown in Table 1. ^{15}O-water is considered to be the most accurate PET flow tracer. Because it is freely diffusible across capillary and cell membranes, extraction is near unity and independent of flow. However, it is not used widely in the clinical routine due to the need for a dedicated cyclotron for continuous production, and the rapid equilibration between blood and tissue prevents acquisition of a myocardial perfusion image for visual interpretation. ^{13}N-ammonia has very high initial extraction (>90% at peak stress) and is well suited for MBF quantification. Tracer retention in the form of ^{13}N-glutamine is somewhat lower, but is still higher than ^{201}Tl and the ^{99m}Tc-labeled SPECT agents.[19] It also requires an onsite cyclotron for production, which can make routine examinations relatively expensive. The ^{18}F-MC-1 inhibitor (e.g., BMS-747158-02) currently entering phase III clinical trial is also

From the National Cardiac PET Centre, University of Ottawa Heart Institute, Ottawa, ON, Canada.
Reprint requests: Robert A. deKemp, PhD, National Cardiac PET Centre, University of Ottawa Heart Institute, 40 Ruskin St., Ottawa, ON K1Y 4W7, Canada; *radekemp@ottawaheart.ca*.
J Nucl Cardiol 2010;17:555–70.
1071-3581/$34.00

doi:10.1007/s12350-010-9256-9

Table 1. Properties of PET blood flow tracers

	^{15}O-water	^{13}N-ammonia	^{82}Rb	^{18}F-MC-1 inhibitor
Extraction fraction at peak stress flow (%)	~100	>90	~40	>90[†]
Retention fraction at peak stress flow (%)	NA	55-65	25-30	?
Isotope half-life (min)[60]	2.03	9.97	1.27	109.8
Injected activity for 3D PET [MBq (mCi)]	700-900 (19-24)	370-550 (10-15)	750-1500 (20-40)	150-300 (4-8)
Rest + stress total dose for 3D PET (mSv)[26-28]	1.6-2.0	1.5-2.2	1.1-2.2	7-10
Rest-stress interval (min)	0	20-40	0	?
MBF (MPI) Scan-time (min)	6 (NA)	2-20 (10)	2-8 (6)	2-10 (?)
RMS positron range (mm)[66]	1.02	0.57	2.60	0.23
Reconstructed image resolution (mm)	8-12	6-10	8-12	4-8
Production method	On-site cyclotron	On-site cyclotron	Generator	Regional cyclotron
FDA approved	No	Yes	Yes	No (phase III)

NA, Not applicable for freely diffusible tracers.
[†]Measured in excised rat hearts.[21]
[?]Data not available.

produced using a cyclotron, but can be transported regionally due to the 2-h half-life of ^{18}F.[20] The initial extraction of this tracer also appears to be very high in animals,[21] although there is limited human data available at this time. Higher count density and a short positron range can produce images with higher reconstructed resolution compared to ^{13}N-ammonia and ^{15}O-water. Rest-stress imaging protocols with the MC-1 inhibitor are complicated somewhat by the long retention of the tracer in myocardium.[20]

The most commonly used cardiac PET perfusion tracer is generator-produced ^{82}Rb which does not require a cyclotron. The short half-life ($t_{1/2}$ = 76.4 seconds) enables fast serial imaging,[22] but relatively low count density requires more reconstruction smoothing, producing images with lower spatial resolution. ^{82}Rb extraction at peak stress flow is substantially lower than ^{13}N-ammonia, and requires a larger correction to estimate MBF from the tracer uptake rate. Due to the short half-life, stress is typically performed using pharmacologic vasodilatation on the scanner bed. Although exercise stress is feasible with ^{82}Rb, routine clinical protocols may be more practical using the ^{18}F-MC-1 inhibitor or ^{13}N-ammonia. ^{82}Rb-chloride has been approved for clinical use by the FDA since 1989, and CMS reimbursed since 1995. Over the past few years, the number of centers in the United States performing ^{82}Rb MPI has been growing exponentially, in part due to the improved accuracy recognized with PET vs SPECT MPI. The costs of ^{82}Rb PET depend on patient throughput, but can be competitive with ^{99m}Tc SPECT imaging, particularly with generators lasting 6-8 weeks for use with 3D PET.[23]

^{82}Rb PET has the greatest immediate potential permitting routine MBF imaging to be integrated into the standard clinical MPI workflow, and will be the focus of this review. However, many concepts developed for robust MBF quantification with ^{82}Rb are also applicable to other PET (and possibly SPECT) tracers.

^{82}Sr/^{82}Rb Generator

Commercial ^{82}Rb generators consist of a tin-oxide column resin loaded with ^{82}Sr ($t_{1/2}$ = 25.5 days), which decays into ^{82}Rb.[23] The column is conditioned to bind Sr, but not Rb. Flushing with physiologic 0.9% saline removes the ^{82}Rb activity in the eluate, while Sr remains bound to the column. Within 6 minutes after flushing the column, more than 95% of the ^{82}Rb activity in the column is replenished, thus allowing repeat ^{82}Rb injections at very short intervals.

Generators are typically supplied with 3700 MBq (100 mCi) of ^{82}Sr activity, enabling the elution of 1500-2200 MBq (40-60 mCi) of ^{82}Rb activity for 2D PET MPI imaging over the useful life of the generator (28 days). With 3D PET acquisitions, 750-1500 MBq

(20-40 mCi) may be used without compromising image quality. Thus, it may be possible to extend the useful life of the generator beyond 4 weeks, and operating costs can be significantly reduced. The primary cost associated with ^{82}Sr/^{82}Rb generator production is the cost of the parent isotope ^{82}Sr. Manufacturers have attempted to reduce this expense by reclaiming residual ^{82}Sr activity from spent generators, or by reloading additional ^{82}Sr activity onto spent generators for repeated use.[23]

^{82}Rb Infusion System

Because of the short half-life of ^{82}Rb, the generator eluate must be infused directly into the patient intravenously (IV) using a dedicated infusion system. Infusers consist of a sterile saline supply that is flushed through the generator and into the patient IV through a sterilizing filter. A computer system monitors the activity eluted from the generator using a radioactivity counter on the patient outlet line and stops the elution when a preset activity has been delivered to the patient. If the saline flow-rate is constant, the ^{82}Rb activity vs time profiles vary as the generator ages (Figure 1A), which alters the delay required for blood clearance and the timing for optimal uptake imaging.[24] With an alternate design including a generator bypass line (Figure 1C), the flow of saline between generator and bypass can be controlled to achieve constant-activity-rate elution profiles that are reproducible throughout the useful life of the generator as shown in Figure 1B.[25] These slow-bolus

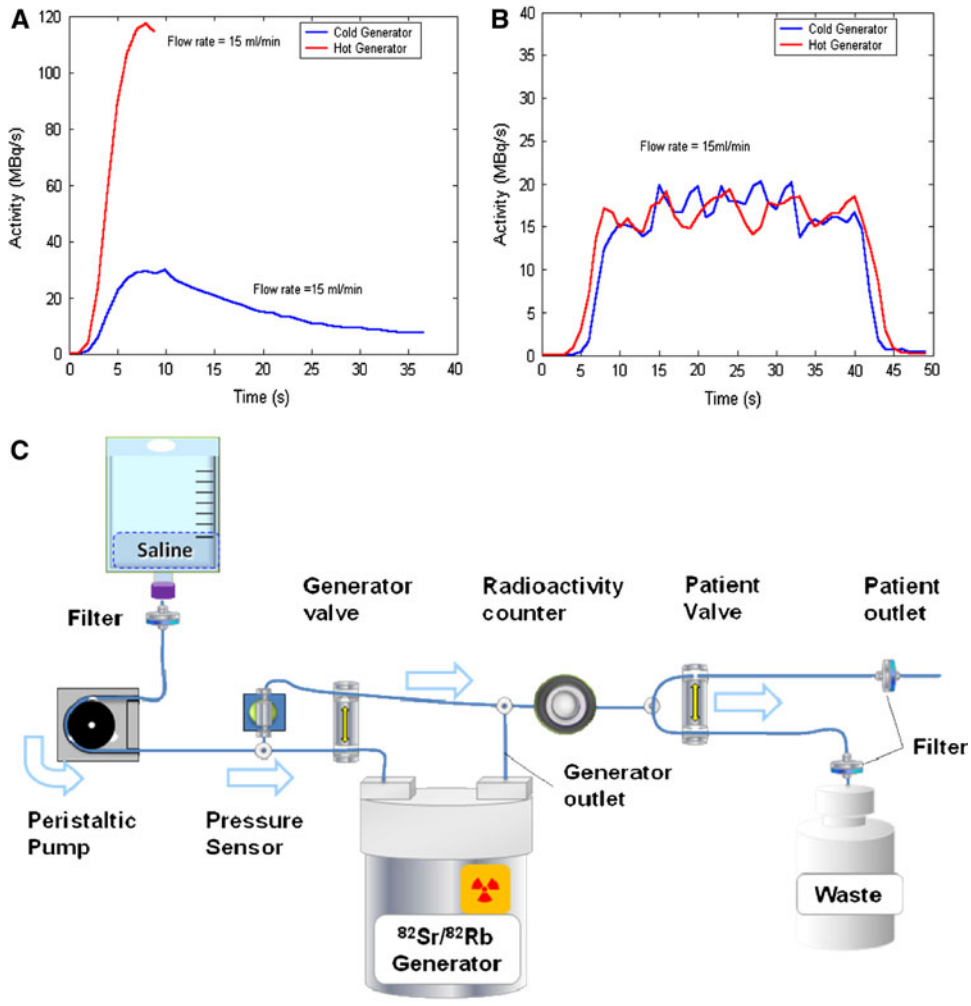

Figure 1. (**A**) (*Left*) Change in time-activity profiles when eluting a new (*red*) and old (*blue*) ^{82}Sr/^{82}Rb generator at a constant flow rate. (**B**) (*Right*) Constant-activity-rate profiles obtained with the alternate system design shown in (**C**). (**C**) Schematic of an alternate design ^{82}Rb infusion system.

infusion methods are particularly useful to limit detector dead-time losses and saturation effects for dynamic imaging with 3D PET systems.

The addition of a generator bypass line also enables flushing of all activity from the patient IV tubing at the end of the elution, thus removing residual activity which contributes to image scatter and detector dead-time during the first-pass transit, particularly with 3D PET.

^{82}Rb Dosimetry

According to the International Commission on Radiological Protection (ICRP 1997), the radiation effective dose from a ^{82}Rb injection is 3.4 mSv/GBq.[26] However, this was a very conservative estimate based on a theoretical blood flow model which does not take into account the actual tracer biodistribution. Human data suggest that the effective dose is on the order of 0.75 mSv/GBq,[27] confirmed recently by our own data measured with dynamic PET/CT.[28] The low effective dose of ^{82}Rb is expected largely due to the ultra-short half-life, similar to ^{15}O-water. ^{13}N-ammonia has a slightly higher effective dose due mainly to its longer half-life. While the effective dose estimates for the MC-1-inhibitor are preliminary, they are expected to be similar to other ^{18}F-labeled compounds.

The use of low-dose CT attenuation correction (CTAC) instead of transmission sources increases the effective patient dose by $\sim$0.5 mSv per scan, depending on the exact technique used. The use of 3D-mode acquisition, on the other hand, can cut the required tracer activity in half, and therefore halves the patient effective dose from the tracer. Total effective dose for a combined rest + stress ^{82}Rb MPI + MBF scan with 3D PET is in the range of 1-2 mSv for a typical injected activity of 10 MBq/kg.

^{82}Rb Biology

^{82}Rb is a potassium analog extracted from the arterial blood by all perfused tissues through passive diffusion and active ion transport by the Na-K-ATPase pump. At rest approximately 50-70% of injected ^{82}Rb is extracted in the first-pass transit through the circulation, and as little as 30-40% at peak stress flows.[29-31] Some ^{82}Rb washout may occur under conditions of acute ischemia or infarction, but typically the tracer reaches a constant level in the myocardium approximately 1.5-2 minutes after injection, enabling static perfusion image acquisition for 4-8 minutes.[32] Uptake and washout rates can be quantified using dynamic imaging for 2-10 minutes from the start of injection. With a properly formulated kinetic model, the uptake rate K_1 (transport from blood to tissue) can be used to estimate absolute MBF (mL/minute/g), using a tracer extraction function calibrated to an appropriate gold-standard such as microspheres,[33] ^{15}O-water,[34] or ^{13}N-ammonia derived flows.[35] Tracer washout rates may be useful for assessing myocardial tissue viability in some acute settings, where nonviable myocardium appears to have an increased rate of ^{82}Rb washout.

IMAGING PROTOCOLS

As shown in Figure 2,[36] a complete MPI exam consists of two scans: one at physiologic rest followed by one at hyperemic stress. Quantification of MBF requires dynamic PET imaging from the start of tracer injection for at least 2 minutes. The short half-life of ^{82}Rb enables repeat imaging of the same patient after only 6 minutes, since the background activity from the previous scan is decayed to below 5%. Longer-lived tracers may require additional time for tracer decay between rest and stress scans to avoid rest contamination of the stress image. The short half-life of ^{82}Rb also requires stressing of the patient on the scanner bed to avoid isotope decay during patient transfer from a treadmill onto the scanner bed. While some have demonstrated exercise-induced stress using an on-bed exercise ergometer,[37] pharmacologic-induced stress is usually preferred, as it is technically easier, is less prone to image artifacts due to patient motion and upward-creep, and can be used to stress patients unable to exercise. Table 2 lists commonly used stress agents and their mechanism of action. The most commonly used methods are Adenosine-based.

PET INSTRUMENTATION

Several recent advances in PET instrumentation are well suited for high-throughput MBF imaging.

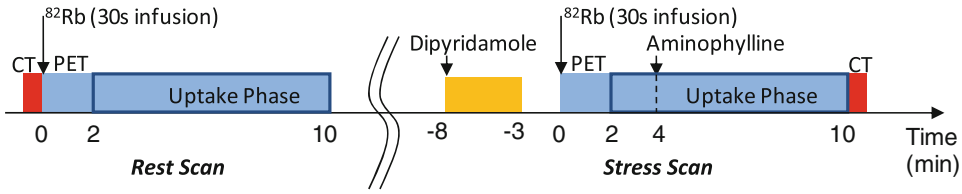

Figure 2. ^{82}Rb image acquisition protocol (from Klein et al, J Nucl Cardiol 2010).[36]

Table 2. Common cardiac stress methods

Method	Mechanism
Exercise	Increased metabolic demand
Dobutamine	Increased sympathetic tone
Cold-pressor	Endothelial dilatation
Dipyridamole ± aminophylline	Vascular smooth muscle (+endothelial) dilatation
Adenosine, ATP, regadenasone	Vascular smooth muscle (+endothelial) dilatation

Faster Detectors

Faster detectors (e.g., LSO/LYSO/LGSO) with high light-output, coupled with fast electronics produce lower dead-time and pile-up losses, with lower random coincidence rates, result in wide dynamic-range and higher peak count-rates, particularly in 3D acquisition mode. These features can translate to reduced image noise during the bolus first-pass transit through the heart. In addition, improved coincidence timing resolution can enable time-of-flight reconstruction to further improve image signal-to-noise ratios, particularly in larger patients with lower recorded count statistics.

For MBF quantification, adequate system accuracy must be maintained over a wide range of count-rates for dynamic imaging of the bolus first-pass through the heart and lungs. Current NEMA standards[38] do not assess high-count-rate accuracy or dynamic-range, but this can be evaluated using a simple cardiac phantom study[39] as shown in Figure 3. This study shows that in the early time frames (high-count-rates), the activity concentration in the heart can be inaccurate due to nonlinearities in the scanner acquisition hardware and/or reconstruction software. In this case, the maximum activity that should be administered to the patient is

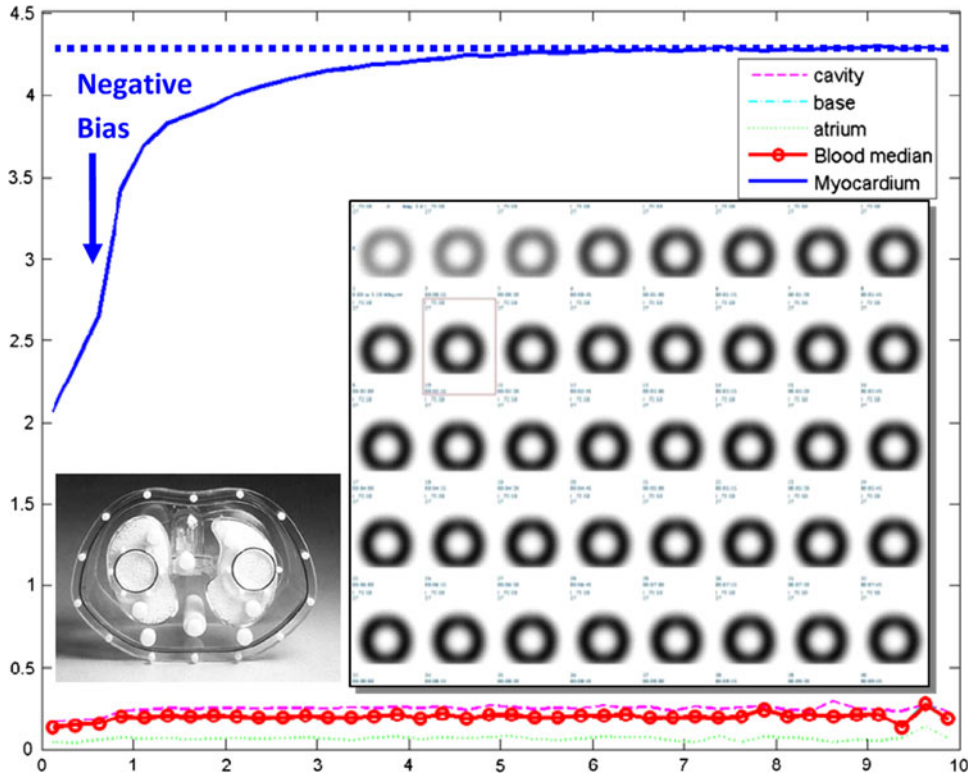

Figure 3. Decay-corrected dynamic images of a heart phantom (inset) filled with 82Rb. The myocardium time-activity-curve demonstrates severe negative bias in the early high-count-rate frames. The dynamic-range with <15% bias extends over two to three orders of magnitude activity from ~1.5 to 10 minutes, where the coincidence dead-time losses are less than ~35%. Images were acquired on a Discovery RX (GEHC) in 3D-mode with 1100 MBq (30 mCi) in the myocardium compartment at time = 0 minutes.

limited, based on the amount of bias that can be tolerated in the early high-count-rate frames.

3D-Mode Acquisition

The 3D-mode acquisition is now standard on most new commercial PET systems. Higher sensitivity compared to 2D-mode acquisitions, combined with accurate 3D scatter correction and effective randoms rejection, enables injected doses to be reduced by a factor of 1.5-2, depending on patient size as shown in (Figure 4). For ^{82}Rb in particular, accurate correction of the prompt gamma background can help to maintain quantitative accuracy in 3D-mode.[40,41]

List-Mode Acquisition

List-mode acquisition enables reconstruction of static, dynamic, ECG- and respiratory-gated images, all with a single injection, and without lengthening the time or increasing the cost of the exam. This feature is essential to permit addition of dynamic first-pass imaging to the standard ECG-gated sequence which has been the clinical standard for many years, permitting simultaneous assessment of MBF as well as the relative perfusion distribution and LV contractile function. During the uptake phase of the scan (starting 1.5-2 minutes after ^{82}Rb infusion), a static uptake image is reconstructed for MPI interpretation. Simultaneous gating of the image with an ECG trigger is used to reconstruct gated images of the beating heart over a similar time period, to interpret contractile function (e.g., wall motion, thickening, and ejection fraction). Finally, a series of dynamic images is reconstructed from the start of tracer injection, to quantify MBF.

The total rest-stress protocol can be completed in 30-40 minutes, depending on the stress protocol (3-8 minutes), dynamic PET imaging time (6-10 minutes), and CTAC scan time (2-30 seconds). With a dedicated camera and experienced staff, it is possible to complete 10-12 patients in a standard work-day.

Iterative Reconstruction

Iterative reconstruction including detector geometry and response modeling, as well as the proper consideration of Poisson count statistics, can result in improved resolution and/or reduced image noise with maintained quantitative accuracy, if fully convergent methods are used.

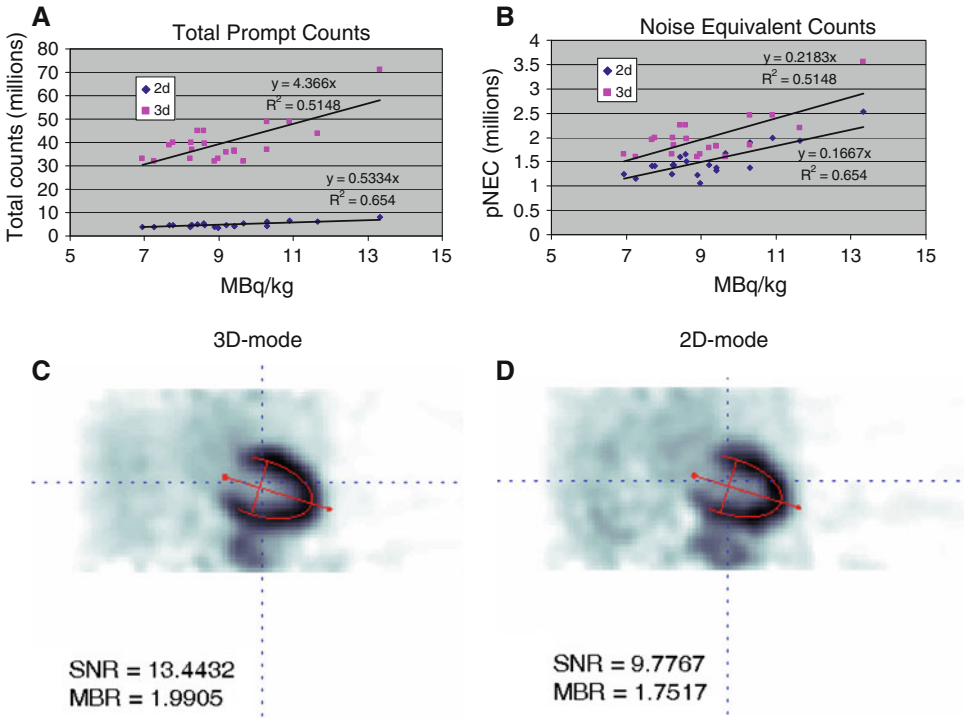

Figure 4. (**A**) Total prompt counts measured from 2.5 to 10 minutes in patients administered 10 ± 1.5 MBq/kg were eight times higher in 3D vs 2D mode on the Discovery RX (GEHC). (**B**) Patient pseudo noise-equivalent counts (pNEC) accounting for the noise effects of random and scattered coincidences, still show a net benefit in counts and SNR in 3D-mode (**C**) vs 2D-mode (**D**) images, both reconstructed with the same filter.

PET and SPECT transaxial images were traditionally reconstructed using filtered back projection, but iterative reconstruction methods have become the new standard, in part due to the introduction of more powerful computers which now make these algorithms feasible in clinical practice. Iterative reconstruction can offer images with improved noise properties, improved myocardium to blood pool contrast, and higher spatial resolution. Alternatively, iterative reconstruction may allow image quality and resolution to be maintained relative to filtered backprojection, but with less tracer activity administered to further decrease the patient dose.

A potential disadvantage to some iterative reconstruction methods is inaccurate global and/or regional quantification, according to the algorithm convergence properties that can depend on the local count statistics and organ activity contrast.[42] While absolute quantification may not be critical for static and gated imaging, it is vital for accurate MBF quantification from dynamic image sequences. Careful consideration must be given to evaluate the convergence properties of iterative algorithms for dynamic imaging and MBF quantification.[42]

^{82}Rb image reconstruction also requires special consideration of the 776.5 keV cascade gamma photon that is emitted with ~15% abundance simultaneously with the positron. This high-energy photon can be scattered and recorded in coincidence with one of the 511 keV annihilation photons. A relatively uniform prompt background activity is produced in this case, which can interfere with accurate scaling of the scatter projections in 3D-mode, if not properly corrected.[41] Due to the higher positron range of ^{82}Rb and lower count statistics, images have generally lower resolution compared to tracers labeled with longer-lived PET isotopes as listed in Table 1.

Combined PET-CT

Combined PET-CT (x-ray computed tomography) can generate noiseless attenuation images in a fraction of the time compared to attenuation imaging with transmission sources. A low-dose (0.1-1.0 mSv) CT attenuation scan requires 2-30 seconds and can shorten the overall protocol duration, compared to isotope transmission scans which typically require 4-10 minutes. The total protocol duration may be further shortened by using a single attenuation image (whether CT or transmission) to correct both rest and stress images. In this case, the patient should not be moved between scans and ideally, the attenuation image acquired between rest and stress scans to minimize inter-scan motion.

If the CT has diagnostic capabilities, it may also be used to perform coronary calcium scoring, CT angiography, and/or gated LV function imaging, all of which may be co-registered with the PET perfusion data. Proper consideration must be given to the effects of respiratory motion for accurate attenuation correction, since the PET data are acquired over many respiratory cycles, whereas a fast CT attenuation scan can be acquired at a single point in the breathing cycle. This respiratory motion mismatch can result in image artifacts and false-positive defects, if not properly accounted for.

Despite the many advantages of PET-CT, dedicated cardiac PET-only systems using conventional coincidence or singles transmission imaging may provide a lower-cost alternative to PET-CT. Such a scanner may have slightly reduced throughput due to longer attenuation scan times, but would avoid some complications of mismatched respiratory motion artifacts from fast CTAC.[43]

REPEATABLE TRACER INFUSION

The infused activity should be adjusted for patient size to compensate for tracer distribution volume in the body and increased attenuation. This ensures sufficient tracer activity in the myocardium during the uptake phase for high-quality MPI. However, for dynamic image acquisition in 3D-mode, the activity must be limited to avoid saturation of the detectors and/or electronics during the first-pass transit through the heart, when the tracer has not had time to decay or to be distributed throughout the body. Low count statistics in the late time frames is especially relevant to ^{82}Rb due to its fast decay. The late time frames may be extended to collect more counts, but beyond 6 minutes, little activity remains. With 2D imaging approximately 20 MBq/kg of ^{82}Rb activity is typically injected, but with 3D imaging as little as 10 MBq/kg may be sufficient, requiring 750-1500 MBq (20-40 mCi) for typical patient sizes.[44]

An alternative method to avoid detector saturation during first-pass imaging, is to lengthen the duration over which the activity is administered, as demonstrated in Figure 5 and the results listed in Table 3.[45] In this canine study performed on a 3D-only scanner (Siemens ECAT ART), sequential ^{82}Rb infusions were performed with varying durations, and dynamic images analyzed to determine regional MBF. The mean MBF measurements were consistent for all infusion durations; however, the estimated parameter variability was reduced almost fourfold, suggesting more highly reproducible quantification. The maximum detector dead-time decreased as the infusion duration increased, suggesting that the camera remained in a more linear range throughout the

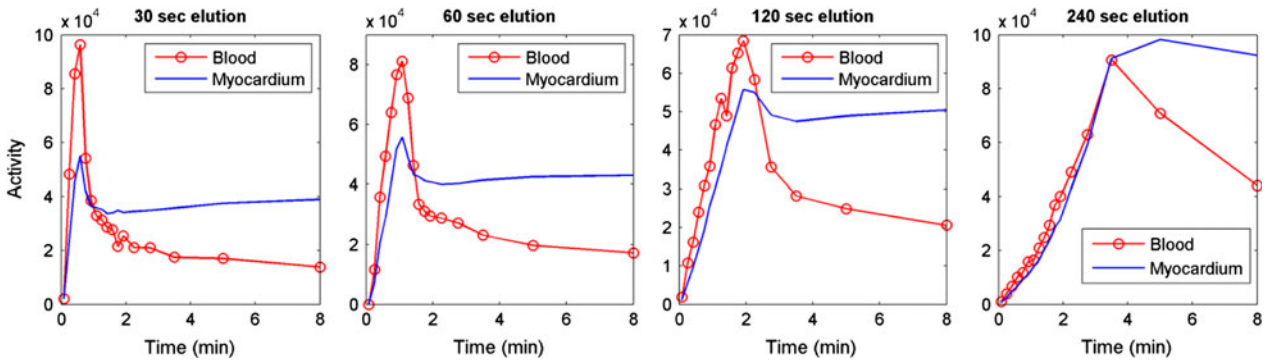

Figure 5. Blood and myocardium TACs with variable duration ^{82}Rb infusions.

Table 3. Improvement in MBF variability with long ^{82}Rb infusions

Infusion duration	30 s	60 s	120 s	240 s
MBF (mL/minute/g)	1.3	1.3	1.2	1.2
±SD/Mean (%)	2.3	2.0	1.3	0.6
Peak count rate (kcps)	215	200	105	65
Dead-time at peak count rate (%)	40	38	27	20

acquisition. Similar techniques may be useful for MBF quantification on 3D PET systems with limited dynamic-range.

IMAGE ANALYSIS

Cardiac images are commonly reoriented to the left ventricle (LV) myocardium reference frame for reporting. Images are viewed as short axis slices (SA), vertical long axis (VLA), and horizontal long axis (HLA). The LV myocardium is segmented and the mid-myocardial activity represented in a polar-map format as demonstrated in Figure 6. Likewise, a blood region of interest (ROI) is defined in the center of the left ventricular and/or atrial cavity. The myocardium and blood ROIs can be sampled in all dynamic time frames to generate the respective TACs for MBF quantification.

MYOCARDIAL BLOOD FLOW QUANTIFICATION

The dynamic exchange of activity between arterial blood and myocardial tissue can be described using the general compartmental model illustrated in Figure 7, where $C_a(t)$ and $C_t(t)$ are the activity concentrations (Bq/cc) as a function of time in the arterial blood and myocardial tissue, respectively. The uptake rate

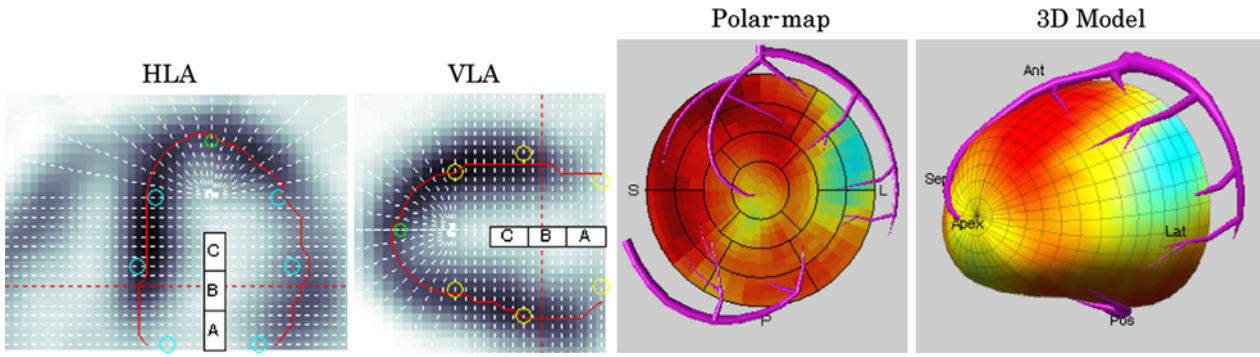

Figure 6. Horizontal and vertical long axis (HLA and VLA, respectively) views of the left ventricle myocardium, and segmentation of the mid-myocardial activity (*red line*). The mid-myocardial activity can be displayed as a polar-map or 3D model of the myocardium.

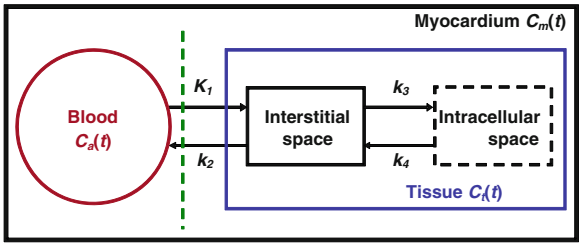

Figure 7. Myocardial compartmental model consisting of blood and tissue and the transport of tracer between compartments.

K_1 (mL/minute/g) describes the transfer of tracer from blood to tissue, while k_2 (min^{-1}) is the washout rate in the opposite direction. While the myocardial tissue may be modeled using subcompartments (interstitial and intracellular), the associated transfer mechanisms may not be identifiable, nor in fact needed for accurate MBF quantification.

Assuming a one-tissue-compartment model (without k_3, k_4), the tracer kinetics can be represented using the differential function shown in Equation 1 or the equivalent convolution operation shown in Equation 2.

$$\frac{dC_t(t)}{dt} = K_1 \cdot C_a(t) - k_2 \cdot C_t(t) \quad (1)$$

$$C_t(t) = K_1 e^{-k_2 t} \otimes C_a(t) \quad (2)$$

The measured time-activity curves (TACs) $C_m(t)$ and $C_a(t)$ are commonly derived from the dynamic image sequence by sampling regions of interests (ROIs) over the myocardium and LV blood cavity, respectively. $C_a(t)$ is assumed to consist of pure arterial blood signal and $C_m(t)$ is assumed to consist of both arterial blood and myocardial tissue signal as shown in Equation 3, where *RC* is referred to as the recovery coefficient and represents the ROI's partial volume associated with myocardial tissue. *FBV* is referred to as the fractional blood volume and represents the ROI's signal associated with arterial blood. In the interventricular septum, there can also be spillover from arterial blood the right ventricle, which may be added into the *FBV* term below.

$$C_m(t) = FBV \cdot C_a(t) + RC \cdot C_t(t) \quad (3)$$

By substitution of Equation 2 into Equation 3, the following kinetic model equation is derived.

$$C_m(t) = FBV \cdot C_a(t) + RC \cdot K_1 e^{-k_2 t} \otimes C_a(t) \quad (4)$$

Since the product of *RC* and K_1 cannot be uniquely solved in this equation, it is commonly assumed that the ROI's total signal recovery consists only of arterial blood or myocardial tissue signal, and therefore $RC = 1 - FBV$, which makes Equation 4 uniquely solvable.

K_1 can be related to flow, *MBF* mL/minute/g, as $K_1 = MBF \times E(MBF)$, where

$$E(MBF) = 1 - e^{-PS/MBF} \quad (5)$$

$E(MBF)$ is a tracer-specific extraction function that accounts for nonlinear tracer extraction as a function of MBF and the effective capillary permeability × surface-area product, *PS* mL/minute/g.[46,47] This model is consistent with the observation that tracer extraction typically decreases with flow, despite the *PS* product increasing due to capillary recruitment. The *PS* function is typically presented using the following form

$$PS(MBF) = \alpha \cdot MBF + \beta \quad (6)$$

By combining Equations 5 and 6, the extraction function is expressed in one of the following forms:

$$E(MBF) = 1 - e^{-(\alpha \cdot MBF + \beta)/MBF} = 1 - a \cdot e^{-\beta/MBF} \quad (7)$$

The extraction function parameters reported in the literature vary somewhat as shown in Table 4 and their corresponding extraction fractions in Figure 8. The extraction of ^{82}Rb is lower than that of water and ammonia, but higher than ^{99m}Tc-Sestamibi and ^{62}Cu-PTSM. Some variability in reported extraction function

Table 4. Reported Renkin-Crone model extraction fraction parameters

Tracer	Citation	*a*	α	β
^{15}O-water	Bergman[67]	0	-	∞
^{13}N-ammonia	Schelbert et al[61]	0.096	2.3	1.083
^{62}Cu-PTSM	Beanlands et al[62]	0.89	0.11	0.45
^{82}Rb	Lortie et al[35]	0.77	0.26	0.63
	Lautamaki et al[63]	0.85	0.16	0.45
	Glatting et al[64] and Schelbert[65]	0.73	0.31	0.593
	Yoshida et al[68]	0.85	0.16	0.45
^{99m}Tc-sestamibi	Leppo and Meerdink[19]	0.87	0.14	0.44
^{201}Tl	Leppo and Meerdink[19]	0.57	0.57	1.02

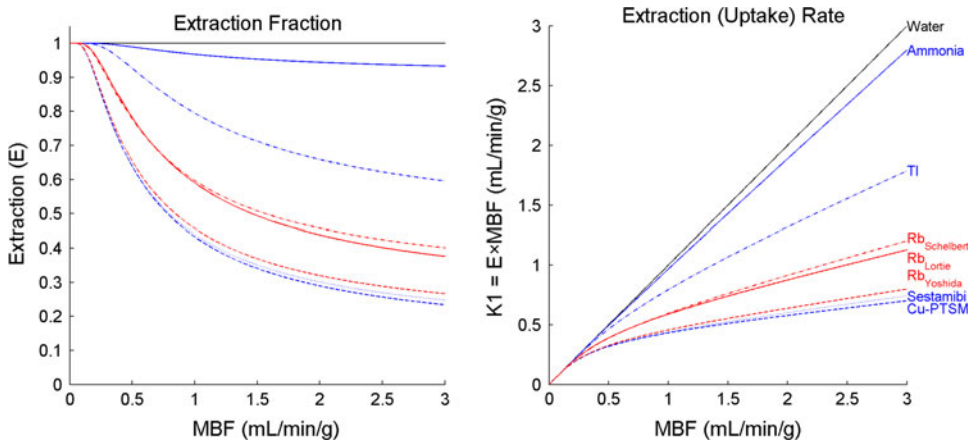

Figure 8. Previously reported extraction function and retention functions for ^{82}Rb compared with other MBF flow tracers.

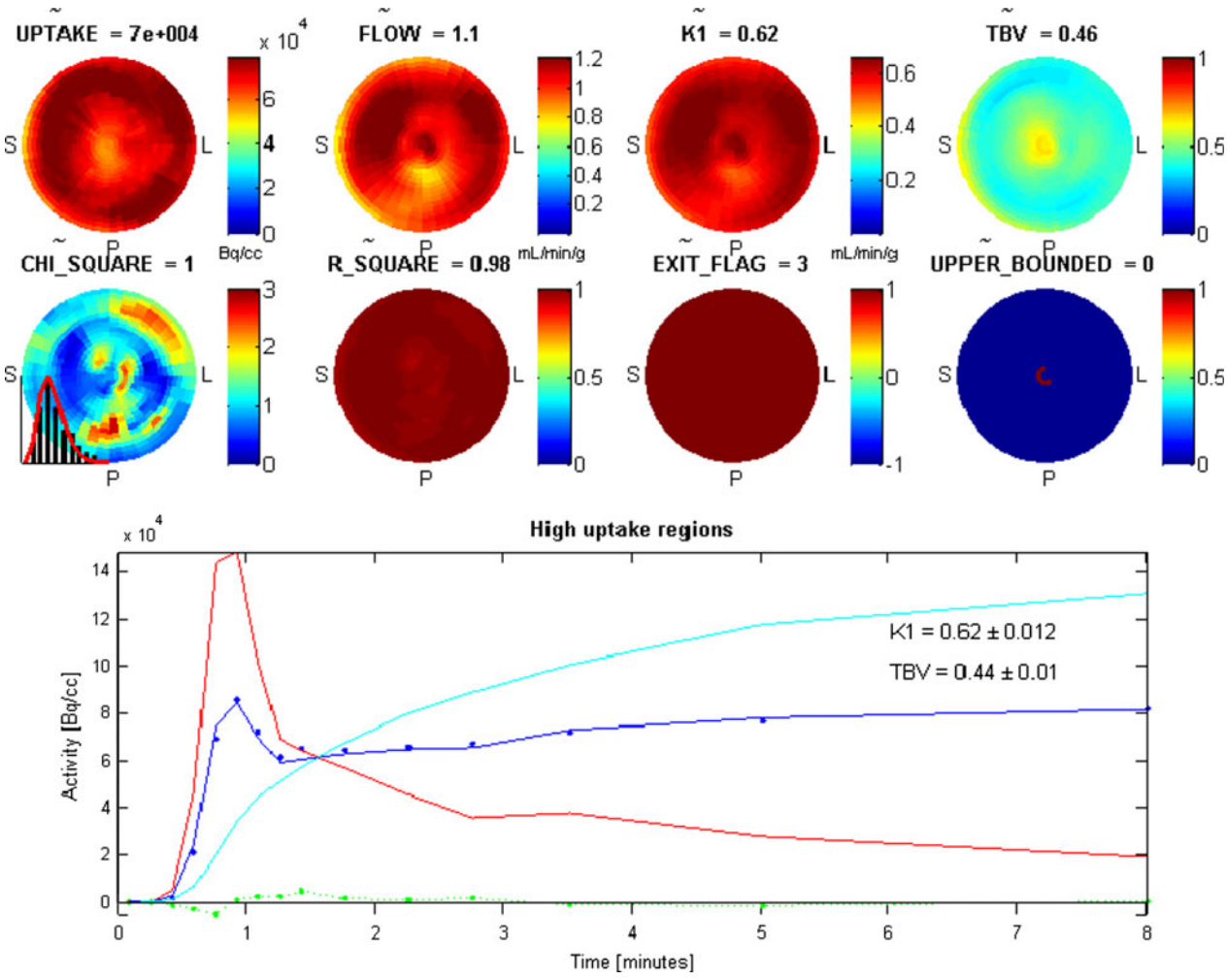

Figure 9. MBF (*flow*) estimation with a 1-tissue-compartment model including regional blood spillover and myocardial recovery (*partial volume*) corrections.

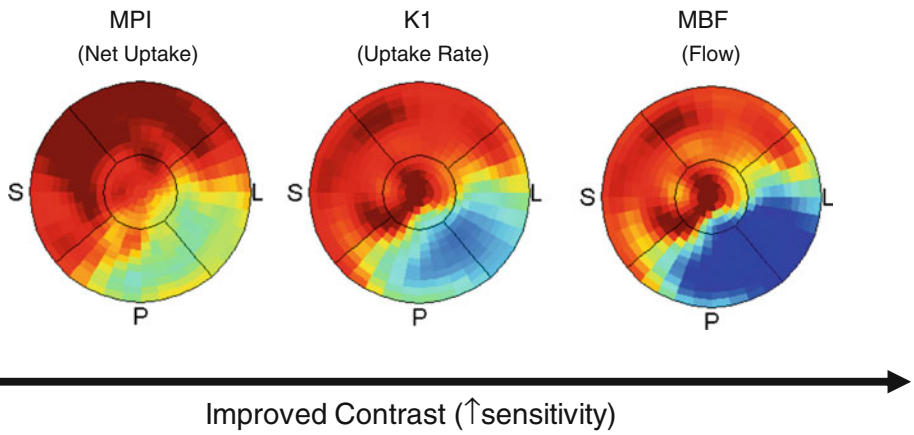

Figure 10. Defect contrast is improved over MPI with ^{82}Rb quantification of the uptake rate (K_1) and MBF, which improves sensitivity.

parameters is due to varying (small) study populations, PET instrumentation, image reconstruction, and analysis methods. Some published functions also include the net effects of tracer washout (k_2), and therefore actually reflect the net tracer retention fraction which is lower than extraction. The extraction functions serve to calibrate MBF estimates to a standard such as ex vivo microspheres or in vivo coronary flow meters or ideal standard tracer.[34]

Global MBF measurements can be derived using a single ROI encapsulating the entire LV myocardium. Alternatively, smaller regions can be segmented to measure MBF regionally as demonstrated in Figure 9. In this case, a regional correction for partial volume loss can help to improve uniformity of normal flow, particularly at the apex. In regions of reduced perfusion, contrast is typically improved with quantification of the tracer uptake rate (K_1), and further amplified following extraction correction, particularly in the low-flow region where the function is the most nonlinear. This is especially useful in patients with poor LV function, where slow blood clearance can reduce defect contrast with standard MPI imaging, subsequently restored with MBF quantification as shown in Figure 10.

PARTIAL VOLUME EFFECTS

The limited resolution of PET as well as cardiac motion results in partial volume averaging that reduce the accuracy of MBF quantification. Partial volume effects reduce the measured activity concentration in the myocardial wall as the resolution decreases, wall thickness decreases, and/or wall motion increases. The apical myocardium, which is thinnest and moves the most, can suffer more severe PV loss and therefore usually has a smaller recovery coefficient (RC) as illustrated in Figure 11.

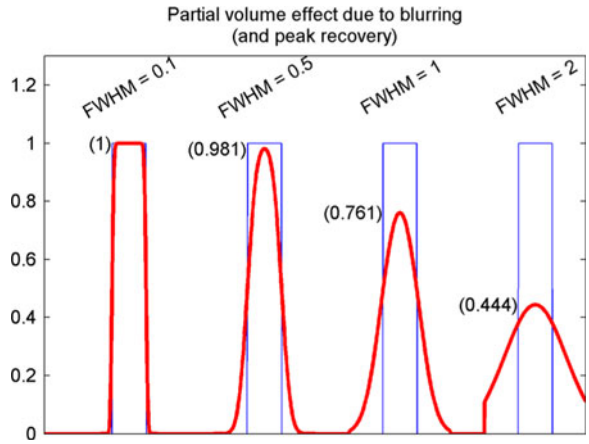

Figure 11. Partial volume averaging due to resolution blurring kernel leads to reduced recovery of peak myocardial image intensity.

Partial volume effects cause spillover of blood signal into the myocardium ROI and vice versa. This results in impure blood and myocardium TACs as demonstrated in Figure 12, where a proportion of blood is evident in the measured myocardium ROI curve as an early peak corresponding to the bolus first-pass through the heart. In the blood, myocardial spillover can result in apparent residual activity in the late time frames, despite complete blood clearance. A blood-to-myocardium spillover model can be used effectively to compensate for regional partial volume losses according to Equation 4 assuming $RC = 1 - FBV$. Myocardium-to-blood spillover can also be compensated in an analogous manner by simultaneous estimation within the ROI model equations,[48-51] or by using factor analysis to estimate pure blood and myocardium signals that are also relatively free of noise.[52-56]

With proper quality assurance and correction for the effects of resolution blurring and tracer extraction,

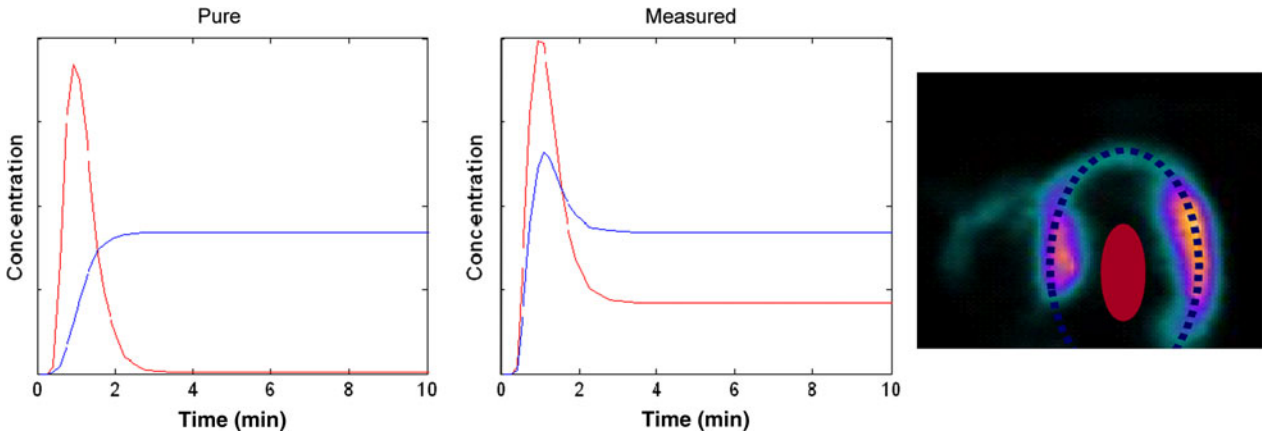

Figure 12. Partial volume spillover effect of blood (*red*) and myocardium (*blue*) TACs.

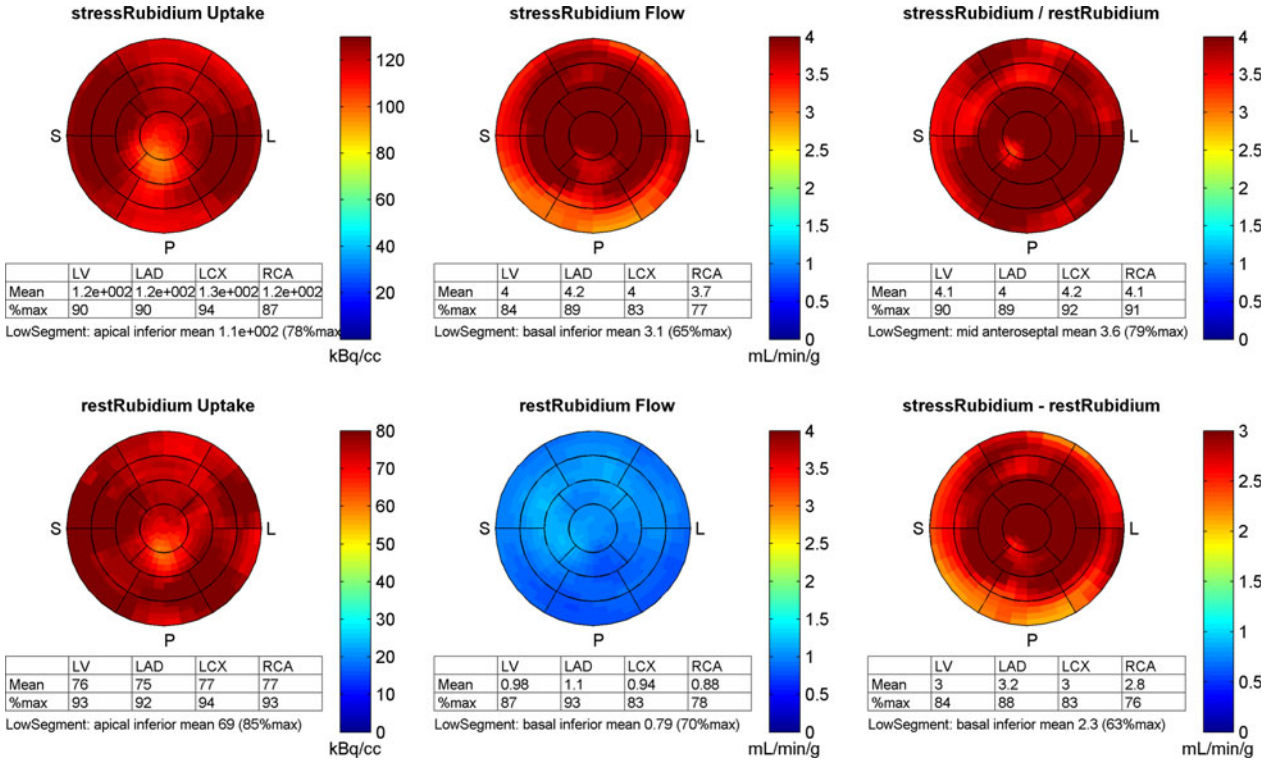

Figure 13. Relative MPI (*uptake*) and absolute MBF (*flow*), flow reserve (stress/rest ratio) and flow increase (stress-rest delta) in a healthy volunteer.

uniform MBF maps are measured with ^{82}Rb in healthy subjects with normal flow reserve (ratio) values around 4, and flow increase (delta) values around 3 mL/minute/g, as shown in Figure 13. Conversely, it is generally accepted that patients with multivessel and/or microvascular disease will typically have flow reserve below 2 and flow delta below 1 mL/minute/g as shown in Figure 14. Accurate coregistration of stress to rest MBF maps is important to avoid artifactual differences appearing in the basal rings of the flow reserve polar maps.

POTENTIAL ARTIFACTS

Attenuation Image Misalignment

Misalignment of PET and attenuation images has been shown to introduce artifacts,[57] particularly at the interface of the myocardium and lung regions (anterolateral wall), which will also be translated directly into the quantitative MBF measurements. These artifacts can be resolved through careful AC quality assurance

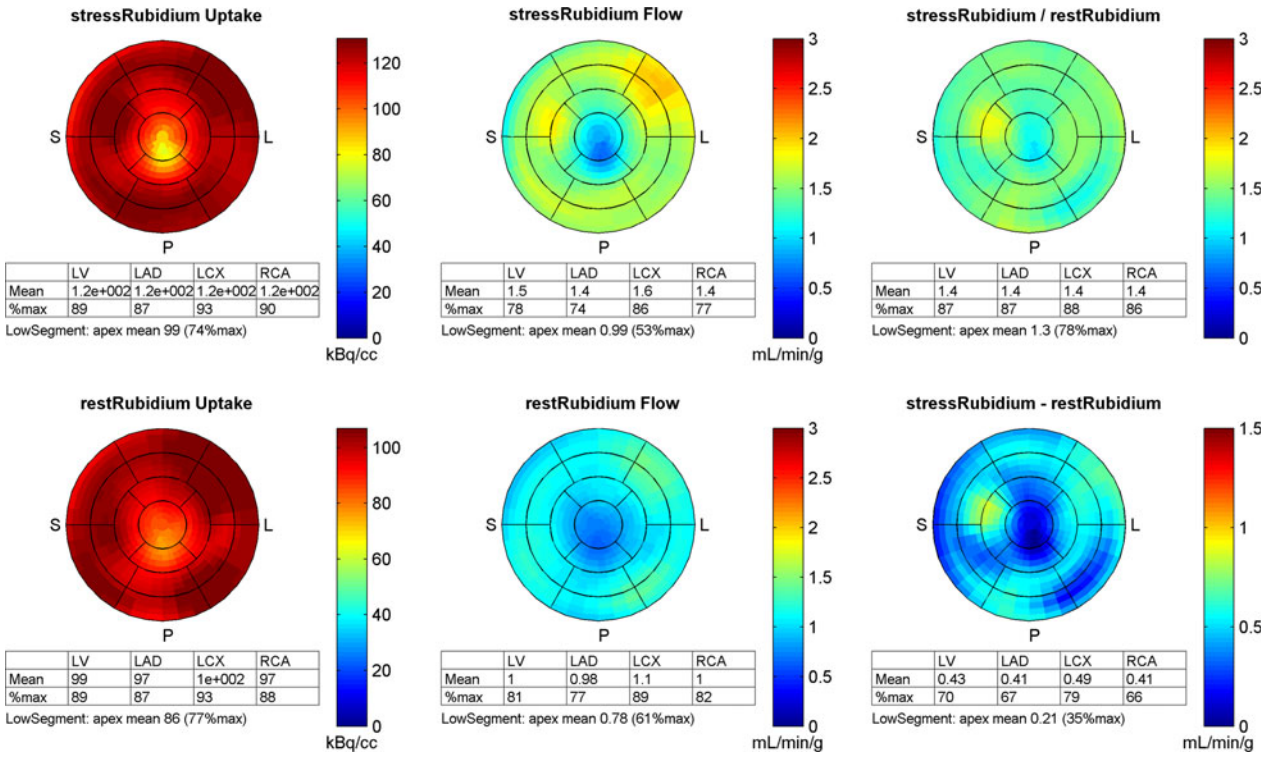

Figure 14. Relative MPI (uptake) and absolute MBF (*flow*), flow reserve (stress/rest ratio) and flow increase (stress-rest delta) in a patient with normal MPI, but impaired flow reserve.

(ACQC) to confirm or correct alignment prior to image reconstruction. CT-based attenuation images are more susceptible to misalignment since they can be acquired very quickly and capture only a snapshot of the diaphragm position within the respiratory cycle and heart wall within the cardiac cycle. Isotope transmission-based attenuation maps are acquired over several minutes and therefore blur the respiratory and cardiac motion equivalent to the emission acquisition. Respiratory motion may be reduced by coaching the patients with shallow breathing or end-expiration breath-holding during the attenuation scan.[43]

The CT-based attenuation map can be susceptible to artifacts from large metal objects in the chest cavity (e.g., pace makers, surgically implanted hardware) and inaccurate attenuation correction can result if CT contrast is present in the LV cavity, therefore CT angiography scans are not typically used for attenuation correction. It may be possible to use low-dose calcium CT scans for attenuation correction, if adequate alignment is confirmed with the PET images.

Extracardiac Spillover

^{13}N-ammonia and the ^{18}F-MC-1-inhibitors can have high retention in the liver, adjacent to the inferior wall of the left ventricle. This can result in significant spillover contamination which may mask relative MPI defects. Liver contamination is typically less severe after MBF quantification with ammonia, when the early scan data (e.g., 0-4 minutes) are used for modeling, because the uptake rate is slower in liver compared to the myocardium. Early ammonia uptake in the lungs can be observed in patients with congestive heart failure, which can complicate proper ACQC alignment and interpretation of both MPI and MBF in the lateral wall.

^{82}Rb images may have high stomach wall uptake apparent at rest, which can also make interpretation of the infero-lateral wall difficult. This can often be resolved by instructing the patient to drink a small carbonated (noncaffeinated) beverage before the rest scan to help distend the stomach wall and reduce the apparent activity near the heart wall.

Patient Motion

A common source of image degradation is patient motion during the dynamic acquisition. In long uptake frames, this is manifest as additional blur in the image, and can be very difficult to detect. With a dynamic image series (for MBF quantification), motion results in misalignment of the time frames leading to artifacts in MBF quantification and regional partial volume correction. While motion cannot be completely avoided, it

can be reduced by minimizing the total scanning time, ensuring patient comfort and some coaching. It should be noted that even arm motion, or twitching of the legs can result in significant chest motion in the axial direction, thus patient cooperation and comfort is extremely important. Ideally, the ACQC alignment should be confirmed and corrected if necessary for each time frame of the dynamic image series independently, but this is not yet feasible in the clinical routine. If significant patient motion is noted during the acquisition, post hoc re-alignment of the dynamic images can be attempted, but in some cases this may not be successful and accurate MBF quantification is not possible.

^{82}Sr/^{82}Rb Generator Costs

The cost of each generator is approximately $US 30,000 and may be used for a standard 28 day period, during which a virtually unlimited number of patients can be examined. The cost-effectiveness of ^{82}Rb PET is therefore, dependent on patient throughput and local reimbursement. The availability of a 6- to 8-week generator for use with low-dose 3D PET, could substantially reduce the cost per scan. Downstream costs such as additional exams and ineffective treatments may also be included in the cost-benefit analysis. Patterson et al[58] have demonstrated the cost-effectiveness of PET using by decreasing the use of invasive coronary angiography and angioplasty procedures. Merhige et al[59] confirmed this finding recently by analyzing downstream resource utilization in a clinical ^{82}Rb PET practice. We are currently performing a multicenter trial to confirm the accuracy and cost-effectiveness of low-dose 3D PET using ^{82}Rb as an alternative radiopharmaceutical for myocardial perfusion imaging (Rb-ARMI) (http://clinicaltrials.gov/).

SUMMARY OF REQUIREMENTS

- Tracer with uptake and retention directly proportional to flow.
  - Low radiation dose, high resolution, and high throughput.
- PET scanner with wide dynamic range.
  - Single injection for MPI (late) and MBF (early) imaging.
  - Combined ECG-gated and dynamic scans with list-mode.
- Validated tracer kinetic model.
  - Regional correction for partial volume effects (PVE).
  - Tracer extraction/retention function.
- Reproducible dynamic image analysis.
  - Low operator variability (automated processing).
  - Quality assurance (CTAC and rest-stress alignment, motion, arterial input, PVC, spillover, model fitting).

CONCLUSION

^{82}Rb PET imaging enables PET centers without access to a cyclotron to perform high-quality ECG-gated MPI and dynamic MBF exams. Since the tracer cost-per-scan decreases with increasing patient volume, the ^{82}Sr/^{82}Rb generator cost is best recovered using a dedicated cardiac PET imaging service. The development of accurate 3D cardiac PET scanners with list-mode capabilities and optimized ^{82}Rb elution systems has made routine MPI and MBF quantification feasible in the clinical setting with reduced dose. While ^{82}Rb MPI using 2D PET is accepted to have increased accuracy over conventional ^{99m}Tc SPECT, additional validation data are needed in the clinical setting using current 3D PET instrumentation. ^{82}Rb with 3D PET imaging is an ultra-low-dose alternative to conventional ^{201}Tl or ^{99m}Tc-based SPECT MPI that also enables high patient throughput and routine assessment of MBF and flow reserve.

Acknowledgments

This work was supported by CIHR grants MOP-79311 and MIS-100935, and Ontario Research Fund Grant RE-02-038. We would like to thank Astellas Pharma US, Inc., Covidien, and GE Healthcare for corporate support to publish and distribute this article. Corporate supporters were not involved in the creation or review of information contained in this article. RK, RB, and RdK receive consulting fees and royalties from DraxImage for the sale of Rb generators. RK and RdK receive profit shares from the sale of FlowQuant.

References

1. Bateman T, Heller G, McGhie A, Friedman J, Case J. Diagnostic accuracy of rest/stress ECG-gated Rb-82 myocardial. J Nucl Cardiol 2006;13:24-33.
2. Go R, Marwick T, MacIntyre W, Saha G, Neumann D, Underwood D, Simpfendorfer C. A prospective comparison of rubidium-82 PET and thallium-201 SPECT myocardial perfusion imaging utilizing a single dipyridamole stress in the diagnosis of coronary artery disease. J Nucl Med 1990;31:1899-905.
3. Stewart R, Schwaiger M, Molina E, Popma J, Gacioch G, Kalus M, Squicciarini S, al-Aouar Z, Schork A, Kuhl D. Comparison of rubidium-82 positron emission tomography and thallium-201 SPECT imaging for detection of coronary artery disease. Am J Cardiol 1999;67:1303-10.
4. Sampson U, Dorbala S, Limaye A, Kwong R, Di Carli M. Diagnostic accuracy of rubidium-82 myocardial perfusion imaging

with hybrid positron emission tomography/computed tomography in the detection of coronary artery disease. J Am Coll Cardiol 2007;49:1052-8.
5. Herrero P, Markham J, Shelton M, Weinheimer C, Bergmann S. Noninvasive quantification of regional myocardial perfusion with rubidium-82 and positron emission tomography. Exploration of a mathematical model. Circulation 1990;82:1377-86.
6. Herrero P, Markham J, Shelton ME, Bergmann SR. Implementation and evaluation of a two-compartment model for quantification of myocardial perfusion with rubidium-82 and positron emission tomography. Circ Res 1992;70:496-507.
7. Yoshinaga K, Katoh C, Noriyasu K, Iwado Y, Furuyama H, Ito Y, Kuge Y, Kohya T, Kitabatake A, Tamaki N. Reduction of coronary flow reserve in areas with and without ischemia on stress perfusion imaging in patients with coronary artery disease: A study using oxygen 15-labeled water PET. J Nucl Cardiol 2003; 10:275-83.
8. Parkash R, deKemp RA, Ruddy TD, Kitsikis A, Hart R, Beauschene L, Williams K, Davies RA, Labinaz M, Beanlands RSB. Potential utility of rubidium 82 PET quantification in patients with 3-vessel coronary artery disease. J Nucl Cardiol 2004;11:440-9.
9. Gould KL. Quantification of coronary artery stenosis in vivo. Circ Res 1985;57:341-53.
10. deKemp RA, Yoshinaga K, Beanlands RSB. Will 3-dimensional PET-CT enable the routine quantification of myocardial blood flow? J Nucl Cardiol 2007;14:380-97.
11. Hutchins GD, Schwaiger M, Rosenspire KC, Krivokapich J, Schelbert H, Kuhl DE. Noninvasive quantification of regional blood flow in the human heart using N-13 ammonia and dynamic positron emission tomographic imaging. J Am Coll Cardiol 1990;15:1032-42.
12. Gerwitz H, Skopicki HA, Abraham SA, Castano H, Dinsmore RE, Alpert NM, Fischman AJ. Quantitative PET measurements of regional myocardial blood flow: Observations in humans with ischemic heart disease. Cardiology 1997;88:62-70.
13. Dayanikli F, Grambow D, Muzik O, Mosca L, Rubenfire M, Schwaiger M. Early detection of abnormal coronary flow reserve in asymptomatic men at high risk for coronary artery disease using positron emission tomography. Circulation 1994;90:808-17.
14. Yoshinaga K, Tamaki N, Ruddy TD, deKemp RA, Beanlands RSB. Evaluation of myocardial perfusion. In: Wahl RL, editor. Principles and practice of PET and PET/CT, ch. 11.1, 2nd ed. Philadelphia, PA, USA: Lippincott Williams & Wilkins; 2009. p. 541-64.
15. Schindler TH, Nitzsche EU, Schelbert HR, Olschewski M, Sayre J, Mix M, Brink I, Zhang X-L, Kreissl M, Magosaki N, Just H, Solzbach U. Positron emission tomography-measured abnormal responses of myocardial blood flow to sympathetic stimulation are associated with the risk of developing cardiovascular events. J Am Coll Cardiol 2005;45:1505-12.
16. Matrougui K. Diabetes and microvascular pathophysiology: Role of epidermal growth factor receptor tyrosine kinase. Diabetes Metab Res Rev 2010;26:13-6.
17. Han B, Baliga R, Huang H, Giannone PJ, Bauer JA. Decreased cardiac expression of vascular endothelial growth factor and redox imbalance in murine diabetic cardiomyopathy. Am J Physiol Heart Circ Physiol 2009;297:H829-35.
18. Fioretto P, Dodson PM, Ziegler D, Rosenson RS. Residual microvascular risk in diabetes: Unmet needs and future directions. Nat Rev Endocrinol 2010;6:19-25.
19. Leppo JA, Meerdink DJ. Comparison of the myocardial uptake of a technetium-labeled isonitrile analogue and thallium. Circ Res 1989;65:632-9.
20. Yu M, Guaraldi MT, Mistry M, Kagan M, McDonald JL, Drew K, Radeke H, Azure M, Purohit A, Casebier DS, Robinson SP. BMS-747158-02: A novel PET myocardial perfusion imaging agent. J Nucl Cardiol 2007;14:789-98.
21. Huisman MC, Higuchi T, Reder S, Nekolla SG, Poethko T, Wester H-J, Ziegler SI, Casebier DS, Robinson SP, Schwaiger M. Initial characterization of an ^{18}F-labeled myocardial perfusion tracer. J Nucl Med 2008;49:630-6.
22. deKemp RA, Ruddy TD, Hewitt T, Dalipaj MM, Aung MT, Beanlands RSB. Detection of serial changes in absolute myocardial perfusion with ^{82}Rb PET. J Nucl Med 2000;41:1426-35.
23. Alvarez-Diez TM, de Kemp RA, Beanlands RS, Vincent J. Manufacture of strontium-82/rubidium-82 generators and quality control of rubidium-82 chloride for myocardial perfusion imaging in patients using positron emission tomography. Appl Radiat Isot 1999;50:1015-23.
24. Epstein NJ, Benelfassi A, Beanlands RS, deKemp RA. A ^{82}Rb infusion system for quantitative perfusion imaging in 3D PET. App Radiat Isot 2004;60:921-7.
25. Klein R, Adler A, Beanlands RS, deKemp RA. Precision-controlled elution of a 82Sr/82Rb generator for cardiac perfusion imaging with positron emission tomography. Phys Med Biol 2007;52:659-73.
26. Valentin J. Radiation dose to patients from radiopharmaceuticals: (Addendum 2 to ICRP Publication 53) ICRP Publication 80. Annals of the ICRP 1998;28(3):1-130.
27. Ryan JW, Harper PV, Stark VS, Peterson EL, Lathrop KA. Radiation absorbed dose estimate for rubidium-82 determined from in vivo measurements in human subjects. In: Proc 4th International Radiopharm Dosimetry Symposium, Oak Ridge Conference 851113; 1986, p. 346-58.
28. Hunter C, Ziadi M, Etele J, Hill J, Beanlands R, deKemp R. New effective dose estimates for Rubidium-82 based on dynamic PET/CT imaging in humans. J Nucl Med 2010;51(S2):1469.
29. Mullani NA, Goldstein RA, Gould KL, Marani SK, Fisher DJ, O'Brien HA, Loberg MD. Myocardial perfusion with rubidium-82. I. Measurement of extraction fraction and flow with external detectors. J Nucl Med 1983;24:898-906.
30. Mullani N, Gould K. First-pass measurements of regional blood flow with external detectors. J Nucl Med 1983;24:577-81.
31. Ziegler W, Goresky C. Kinetics of rubidium uptake in the working dog heart. Circ Res 1971;29:208-20.
32. Weinberg IN, Huang SC, Hoffman EJ, Araujo L, Nienaber C, Grover-McKay M, Dahlbom M, Schelbert H. Validation of PET-acquired input functions for cardiac studies. J Nucl Med 1988;29:241-7.
33. Lekx KS, deKemp RA, Beanlands RSB, Wisenberg G, Wells RG, Stodilka RZ, Lortie M, Klein R, Zabel P, Kovacs MS, Sykes J, Prato FS. Quantification of regional myocardial blood flow in a canine model of stunned and infarcted myocardium: Comparison of rubidium-82 positron emission tomography with microspheres. Nucl Med Commun 2010;31:67-74.
34. Prior J, Allenbach G, Valenta I, Modolo L, Kosinski M, Malterre J, Burger C, Verdun F, Bischof Delaloye A, Kaufmann P. Myocardial blood flow quantitation using Rb-82: Validation to *O*-15-water in healthy volunteers and CAD patients. J Nucl Med 2008;49:74P.
35. Lortie M, Beanlands RSB, Yoshinaga K, Klein R, DaSilva JN, deKemp RA. Quantification of myocardial blood flow with 82Rb dynamic PET imaging. Eur J Nucl Med Molec Imag 2007;34: 1765-74.
36. Klein R, Renaud JM, Ziadi MC, Thorn SL, Adler A, Beanlands RSB, deKemp RA. Intra- and inter-operator repeatability of myocardial blood flow and myocardial flow reserve measurements

using rubidium-82 PET and a highly automated analysis program. J Nucl Cardiol. doi:10.1007/s12350-010-9225-3.
37. Wyss CA, Koepfli P, Mikolajczyk K, Burger C, von Schulthess GK, Kaufmann PA. Bicycle exercise stress in PET for assessment of coronary flow reserve—Repeatability and comparison with adenosine stress. J Nucl Med 2003;44:146-54.
38. Performance measurements of Positron Emission Tomographs (PETs) by the Association of Electrical and Medical Equipment Manufacturers, www.nema.org, 2010.
39. deKemp RA, Klein R, Renaud J, Alghamdi A, Lortie M, DaSilva JN, Beanlands RS. 3D list-mode cardiac PET for simultaneous quantification of myocardial blood flow and ventricular function. In: Nucl Sci Symp and Med Imag Conf Record; 2008. p. 5215-8.
40. Hsu B, Casey ME, Watson CC, Bateman TM, Case JA. Validation of Prompt Gamma Correction for 3D Rb-82 Myocardial Perfusion PET/CT Imaging. J Nucl Card 2008;15:S4.
41. Esteves FP, Nye JA, Khan A, Folks RD, Halkar RK, Garcia EV, Schuster DM, Lerakis S, Raggi P, Votaw JR. Prompt-gamma compensation in Rb-82 myocardial perfusion 3D PET/CT. J Nucl Cardiol 2009;17:247-53.
42. Boellaard R, van Lingen A, Lammertsma AA. Experimental and clinical evaluation of iterative reconstruction (OSEM) in dynamic PET: Quantitative characteristics and effects on kinetic modeling. J Nucl Med 2001;42:808-17.
43. Cook RAH, Carnes G, Lee T-Y, Wells RG. Respiration-Averaged CT for Attenuation Correction in Canine Cardiac PET/CT. J Nucl Med 2007;48:811-8.
44. Dilsizian V, Bacharach SL, Beanlands RS, Bergmann SR, Delbeke D, Gropler RJ, Knuuti J, Schelbert HR, Travin MI. ASNC imaging guidelines for nuclear cardiology procedures: PET myocardial perfusion and metabolism clinical imaging. J Nucl Cardiol. doi: 10.1007/s12350-009-9094-9.
45. deKemp RA, Klein R, Lortie M, Beanlands R. Constant-activity-rate infusions for myocardial blood flow quantification with 82Rb and 3D PET. In: Nucl Sci Symp and Med Imag Conf Record; 2006, p. 3519-21.
46. Renkin EM. Transport of potassium-42 from blood to tissue isolated mammalian skeletal muscles. Am J Physiol 1959;197:1205-10.
47. Crone C. Permeability of capillaries in various organs as determined by use of the indicator diffusion method. Acta Physiol Scand 1963;58:292-305.
48. Katoh C, Morita K, Shiga T, Kubo N, Nakada K, Tamaki N. Improvement of algorithm for quantification of regional myocardial blood flow using 15O-water with PET. J Nucl Med 2004;45:1908-16.
49. Iida H, Kanno I, Takahashi A, Miura S, Murakami M, Takahashi K, Ono Y, Shishido F, Inugami A, Tomura N. Measurement of absolute myocardial blood flow with $H_2^{15}O$ and dynamic positron-emission tomography. Strategy for quantification in relation to the partial-volume effect. Circulation 1988;78:104-15.
50. Iida H, Yokoyama I, Agostini D, Banno T, Kato T, Ito K, Kuwabara Y, Oda Y, Otake T, Tamura Y, Tadamura E, Yoshida T, Tamaki N. Quantitative assessment of regional myocardial blood flow using oxygen-15-labelled water and positron emission tomography: A multicentre evaluation in Japan. Eur J Nucl Med 2000;27:192-201.
51. Manabe O, Yoshinaga K, Katoh C, Naya M, deKemp RA, Tamaki N. Repeatability of rest and hyperemic myocardial blood flow measurements with 82Rb dynamic PET. J Nucl Med 2009;50:68-71.
52. El Fahkri G, Sitek A, Guerin B, Kijewski MF, Di Carli MF, Moore SC. Quantitative dynamic cardiac ^{82}Rb PET using generalized factor and compartment analyses. J Nucl Med 2005;8:1264-71.
53. El Fakhri G, Kardan A, Sitek A, Dorbala S, Abi-Hatem N, Lahoud Y, Fischman A, Coughlan M, Yasuda T, Di Carli MF. Reproducibility and accuracy of quantitative myocardial blood flow assessment with ^{82}Rb PET: Comparison with ^{13}N-ammonia PET. J Nucl Med 2009;50:1062-71.
54. Wu H-M, Hoh CK, Choi Y, Schelbert HR, Hawkins RA, Phelps ME, Huang S-C. Factor analysis for extraction of blood time-activity curves in dynamic FDG-PET studies. J Nucl Med 1995;36:1714-22.
55. Wu H-M, Hoh CK, Buxton DB, Kuhle WG, Schelbert HR, Choi Y, Hawkins RA, Phelps ME, Huang S-C. Quantification of myocardial blood flow using dynamic nitrogen-13-ammonia PET studies and factor analysis of dynamic structures. J Nucl Med 1995;36:2087-93.
56. Klein R, Beanlands RS, Wassenaar RW, Thorn S, Lamoureux M, DaSilva JN, Adler A, deKemp RA. Model based factor analysis of dynamic sequences of cardiac positron emission tomography. Med Phys 2010; in press.
57. Gould KL, Pan T, Loghin C, Johnson NP, Guha A, Sdringola S. Frequent diagnostic errors in cardiac PET/CT due to misregistration of CT attenuation and emission PET images: A definitive analysis of causes, consequences, and corrections. J Nucl Med 2007;48:1112-21.
58. Patterson PE, Eisner RL, Horowitz SF. Comparison of cost-effectiveness and utility of exercise ECG, single photon emission computer tomography, positron emission tomography, and coronary angiography for diagnosis of coronary artery disease. Circulation 1995;91:54-65.
59. Merhige ME, Breen WJ, Shelton V, Houston T, D'Arcy BJ, Perna AF. Impact of myocardial perfusion imaging with PET and (82)Rb on downstream invasive procedure utilization, costs, and outcomes in coronary disease management. J Nucl Med 2007;48:1069-76.
60. Cherry S, Dahlbom M. PET: Physics, instrumentation, and scanners. In: Phelps M, editor. PET molecular imaging and its biological. New York: Springer-Verlag; 2004. p. 1-124.
61. Schelbert HR, Phelps ME, Huang SC, MacDonald NS, Hansen H, Selin C, Kuhl DE. N-13 Ammonia as an indicator of myocardial blood flow. Circulation 1981;63:1259-72.
62. Beanlands RSB, Muzik O, Mintun M, Mangner T, Lee K, Petry N, Hutchins GD, Schwaiger M. The kinetics of copper-62-PTSM in the normal human heart. J Nucl Med 1992;33:684-90.
63. Lautamaki R, George RT, Kitagawa K, et al. Rubidium-82 PET-CT for quantitative assessment of myocardial blood flow: Validation in a canine model of coronary artery stenosis. Eur J Nucl Med Mol Imaging 2009;36:576-86.
64. Glatting G, Bergmann KP, Stollfuss JC, Weismueller P, Kochs M, Hombach V, Reske SN. Myocardial Rb extraction fraction: Determination in humans. J Am Coll Cardiol 1995;25:364A-5A.
65. Schelbert HR. Positron emission tomography of the heart: methodology, findings in the normal and the disease heart, and clinical applications. In: Phelps ME, editor. PET: molecular imaging and its biological applications. New York: Springer.
66. Lecomte R. Technology challenges in small animal PET imaging. Nucl Instrum Meth Phys Res A 2004;527:157-65.
67. Bergmann SR, Fox KA, Rand AL, McElvany KD, Welch MJ, Markham J, Sobel BE. Quantification of regional myocardial blood flow in vivo with H215O. Circulation 1984;70:724-33.
68. Yoshida K, Mullani N, Gould KL. Coronary flow and flow reserve by PET simplified for clinical applications using rubidium-82 or nitrogen-13-ammonia. J Nucl Med 1996;37:1701-12.